Protonation of Lysine Residues Inverts Cation/Anion Selectivity in a Model Channel

Vitali Borisenko,* Mark S. P. Sansom,[†] and G. Andrew Woolley*

*Department of Chemistry, University of Toronto, Toronto M5S 3H6, Canada, and [†]Laboratory of Molecular Biophysics, Department of Biochemistry, University of Oxford, Oxford OX1 3QU, United Kingdom

ABSTRACT   A dimeric alamethicin analog with lysine at position 18 in the sequence (alm-K18) was previously shown to form stable anion-selective channels in membranes at pH 7.0 [Starostin, A. V., R. Butan, V. Borisenko, D. A. James, H. Wenschuh, M. S. Sansom, and G. A. Woolley. 1999. *Biochemistry.* 38:6144–6150]. To probe the charge state of the conducting channel and how this might influence cation versus anion selectivity, we performed a series of single-channel selectivity measurements at different pH values. At pH 7.0 and below, only anion-selective channels were found with $P_{K^+}/P_{Cl^-} = 0.25$. From pH 8–10, a mixture of anion-selective, non-selective, and cation-selective channels was found. At pH > 11 only cation-selective channels were found with $P_{K^+}/P_{Cl^-} = 4$. In contrast, native alamethicin-Q18 channels (with Gln in place of Lys at position 18) were cation-selective ($P_{K^+}/P_{Cl^-} = 4$) at all pH values. Continuum electrostatics calculations were then carried out using an octameric model of the alm-K18 channel embedded in a low dielectric slab to simulate a membrane. Although the calculations can account for the apparent pK_a of the channel, they fail to correctly predict the degree of selectivity. Although a switch from cation- to anion-selectivity as the channel becomes protonated is indicated, the degree of anion-selectivity is severely overestimated, suggesting that the continuum approach does not adequately represent some aspect of the electrostatics of permeation in these channels. Side-chain conformational changes upon protonation, conformational changes, and deprotonation caused by permeating cations and counterion binding by lysine residues upon protonation are considered as possible sources of the overestimation.

INTRODUCTION

Selectivity in ion channels must arise as a consequence of the energetics and kinetics of interactions among the ions, the channel, and water. Recent progress in the determination of channel structures has provided some insight into the origins of cation-selectivity in channels (Doyle et al., 1998; Moczydlowski, 1998). As yet, however, no anion-selective channel structures have been determined at high resolution [although, see Malashkevich et al. (1996) for an intriguing possible motif]. Although an anion-selectivity-determining primary sequence motif has been proposed (Fahlke et al., 1997) and residues critical for anion-selectivity have been identified in several systems (Cescatti et al., 1991; Corringer et al., 1999; Guinamard and Akabas, 1999; Hancock and Benz, 1986; Van Gelder et al., 1997; Wang et al., 1999) the physical origins of anion-selectivity remain unclear.

It has been suggested that the polypeptide backbone of proteins may act as an anion-selectivity filter (Corringer et al., 1999; Tabcharani et al., 1997). This would presumably involve interaction of anions with the positive end of backbone amide dipoles and the substitution of water-anion H-bonding by anion-NH (backbone) H-bonding. Halide complexation via H-bonding has been demonstrated in artificial receptors in nonaqueous solvents (Bell, 1998; Boerrigter et al., 1998). However, thermodynamic data indicate the transfer of K^+ from water to formamide (a model of the polypeptide backbone that is capable of H-bonding) is a favorable process ($\Delta G = -4$ kJ/mol, $\Delta H = -17.9$ kJ/mol), whereas transfer of Cl^- is unfavorable ($\Delta G = +14$ kJ/mol, $\Delta H = +3.5$ kJ/mol) (Cox et al., 1974; Dorman et al., 1996; Marcus, 1997). Thus, if backbone interactions are responsible for anion versus cation (i.e., charge-selectivity), the carbonyl oxygen atoms of the backbone must presumably be sequestered by the structure of the selectivity filter to prevent their interaction with cations.

The literature of molecular recognition is replete with examples where cation/anion selectivity is accomplished via electrostatic interactions (Schmidtchen and Berger, 1997). These interactions are pH-sensitive, can occur without dehydration of the ions, and are relatively insensitive to the detailed three-dimensional structure of the groups involved. In proteins, lysine, arginine, and histidine residues are obvious candidates for electrostatic selectivity determinants. Several anion-binding sites on proteins have been structurally characterized and have been found to contain these residues (Lanyi et al., 1990; Perutz et al., 1994). In the cystic fibrosis transmembrane conductance-regulator chlo-

ride channel, for instance, Arg-352 has been shown to be a major determinant of cation/anion selectivity (Guinamard and Akabas, 1999). pH-dependent changes in channel cation/anion selectivity have been attributed to lysine residues in channels formed by α-toxin (Cescatti et al., 1991) and the porin PhoE (Darveau et al., 1984). Indeed, electrostatic cation/anion selectivity mechanisms appear to operate in a variety of porin channels (Dutzler et al., 1999; Hancock and Benz, 1986; Karshikoff et al., 1994; Schmid et al., 1998), the voltage-dependent anion channel of mitochondria (Bowen et al., 1985), and, to some extent, in the nicotinic acetylcholine receptor channel family (Wang et al., 1999).

We have focused on understanding the cation/anion selectivity properties of the relatively simple channel formed by the peptide alamethicin (Cafiso, 1994; Sansom, 1993a). Alamethicin channels are helix bundles composed of membrane-spanning peptides arranged in parallel (Woolley and Wallace, 1992). We have argued previously that the cation/anion selectivity of alamethicin channels is likely to be dominated by long-range electrostatic interactions (Levitt, 1991a,b). Such interactions can be described by a Poisson–Boltzmann model (Honig and Nicholls, 1995; Warshel and Papazyan, 1998; Weetman et al., 1997).

Numerical solutions of the Poisson–Boltzmann equation can provide a calculated electrostatic energy profile for a cation (or anion) along a trajectory through the pore, if a suitable structural model of the pore is available (Dieckmann et al., 1999; Karshikoff et al., 1994; Sansom, 1998). Detailed structural models of the alamethicin channel have been developed previously (Breed et al., 1997; You et al., 1996). Calculations using these models identified electrostatic features that might act as a source of cation/anion selectivity and led to the design of an alamethicin analog with a lysine residue at position 18 that was predicted to show anion-selectivity. Microscopic (single-channel) measurements showed that alm-K18 channels had reversed cation/anion selectivity when compared to native (alm-Q18) channels at pH 7.0 (Starostin et al., 1999).

Although an isolated lysine residue is expected to have a pK_a of $\sim$10.5 and so is expected to be protonated at pH 7, it is not clear to what extent a ring of lysine residues in a helix bundle channel will be protonated at neutral pH. Because the degree of protonation is expected to affect the cation/anion selectivity of the channel, it was of interest to examine the pH-dependence of channels formed by alm-K18 peptides. We investigated the cation/anion selectivity of channels formed by alm-K18 dimers as a function of pH by making single-channel measurements of reversal potentials in a KCl gradient. In addition, macroscopic measurements of the pH-dependence of channel formation in symmetrical KCl solutions were carried out. Finally the charge state of the channels was examined theoretically by carrying out electrostatic calculations to estimate pK_a of the lysines in model structures of the channels.

EXPERIMENTAL

Materials

Alm-K18 and alm-Q18 (BAPHDA) dimers were prepared as described previously (Starostin et al., 1999). Diphytanoyl phosphatidylcholine was purchased from Avanti Polar Lipids Inc. (Alabaster, AL). Decane, KCl, and the buffers BES, CAPS, CAPSO, TRIZMA, and potassium phosphate, were obtained from Sigma Aldrich Canada (Oakville, ON).

Single-channel measurements

Peptides ($\sim$0.1 μM in methanol) were added to one side (ground potential) of membranes formed from diphytanoyl phosphatidylcholine/decane (50 mg/ml). Polystyrene bilayer chambers with 150-μm apertures (Warner Instrument Co.) were used. Currents were measured and voltage was set using an Axopatch 1D patch-clamp amplifier (Axon Instruments) controlled by Synapse (Synergistic Research Systems) software. A CV-4B-0.1/100 switchable headstage was used, with the headstage gain set at 0.1. Data were filtered at 1 kHz, sampled at 5$\times$ the filter frequency, stored directly to disk, and analyzed using Synapse and Igor (Wavemetrics, Inc.) software. All measurements were made at 22°C ($\pm$2°C). Salt solutions were connected via agarose/ KCl salt bridges to KCl (1 M) reservoirs containing silver/silver chloride electrodes. All KCl solutions (1.3 or 0.01 M KCl) contained 5 mM buffer. Buffers used were as follows: potassium phosphate (pH = 3.0), BES (pH = 7.0), Tris (pH = 8.0), CAPSO (pH = 9.0, pH = 9.55), and CAPS (pH = 10.3, pH = 10.55, pH = 10.8, pH = 11.1). The desired pH was obtained by the addition of potassium hydroxide or hydrogen chloride to the buffered solution as required.

Single-channel current–voltage (I–V) curves were obtained using the following voltage-clamp protocol: a step from 0 to +200 mV, holding at 200 mV for 100–700 ms, then a ramp to −200 mV over the course of 30–80 ms, followed by a return to 0 mV for several seconds. Capacitive currents obtained when no channels opened were subtracted from currents obtained with a single channel open during the ramp. With ramp times ≥20 ms and the amplifier settings described above, the capacitive transient did not lead to amplifier saturation.

This protocol measured the I–V relationship for channels oriented with their N-terminus at the high-salt side of the membrane, because the high-salt (1.3 M KCl) side was always at electrical ground and the N-terminus inserts through the membrane from the side made positive by the applied field (Rink et al., 1994; Woolley et al., 1997). Figures show several individual ramps (I–V curves) superimposed. The ramps have not been averaged or smoothed (except by the amplifier filter) so that the variability and noise shown in the plots directly represents the experimental variability. The number of ramps (n) superimposed in each case is indicated in the figure legends. Smooth curves are drawn through the points in some cases as a visual aid only. Transitions to closed states occurred toward the ends of the ramps but did not occur synchronously and have been removed for clarity.

Multichannel measurements

Macroscopic I–V measurements were made using the same apparatus as described for single-channel measurements; 1 M KCl solutions with 5 mM buffer (potassium phosphate [pH = 3.0] or BES [pH = 7.0] or CAPS [pH = 11.1]) were present on both sides of the membrane. For each pH, an identical volume (40 μL) of a stock solution of the peptide (alm-K18 or alm-Q18) was added to the test side of the membrane. The voltage ramp protocol was simply a linear ramp from 0 to +200 mV over the course of 10 s with holding at 0 mV for 30 s or longer between ramps. Current records from ≥25 voltage ramps were averaged to generate the macroscopic I–V curves shown. Threshold voltages were calculated as the voltage required to generate a conductance of 10 nS. The concentrations of

the stock solutions of alm-K18 and alm-Q18 were different so that the threshold voltages of the two peptides are not directly comparable.

Generation of channel models

Alamethicin models were generated by restrained molecular dynamics simulations as described previously (Breed et al., 1997; You et al., 1996). These simulations were carried out using Xplor V3.1 (Brunger, 1992) with the Charmm param19 parameter set (Brooks et al., 1983). Only polar hydrogens were treated explicitly; apolar groups were represented as extended atoms. The analysis was restricted to models containing eight helices (four alm-K18 dimers). Briefly, an in vacuosimulated annealing protocol (Nilges and Brunger, 1993) was used to grow the atoms of a model out from a predefined Cα template, corresponding to a parallel bundle of alamethicin-K18 helices with C-terminal linkers. Five independent structures were generated at this stage, and each structure was then subjected to five molecular dynamics runs as described in detail in You et al. (1996). A scale factor (0.4) was applied to polar side chain partial charges to mimic the effect of electrostatic screening by pore water and counterions (see Discussion). This procedure led to an ensemble of 25 structures that were subsequently used in electrostatics calculations. Channel pore radius profiles were calculated using the program HOLE (Smart et al., 1993, 1997).

Electrostatics calculations

All electrostatics calculations were made using UHBD version 5.1 (Davis et al., 1991) (with some local modifications) and partial atomic charges from the Quanta/Charmm22 parameter set. Electrostatics calculations were carried out using the procedure described in detail in Adcock et al. (1998). The method follows those developed earlier (Bashford and Karplus, 1990; Honig and Nicholls, 1995) and involves numerical solution of the linearized Poisson–Boltzmann equation. The model system consisted of a low dielectric slab of thickness ~40 Å, into which an alm-K18 channel structure was inserted. The slab was generated from dummy atoms on a simple cubic lattice with a 2.5-Å spacing. The boundary of the protein and low dielectric slab was defined by the solvent-accessible surface, and the dielectric constant (ϵ_{prot}) was set at 4, 10, or 20 as noted in the figure legends. Both the dielectric inside the model pore (representing solvent) and the bulk solvent dielectric were set at 78. A Stern radius of 2 Å was used. Ionic strengths are given in the text and figure legends. A value of 10.5 was used for the pK_a of an unperturbed lysine residue.

To calculate electrostatic potential profiles for permeating ions, a trajectory through the channel was defined using the program HOLE (Smart et al., 1997). Because the channel is relatively wide and straight, this trajectory corresponded roughly to the channel's z axis. The electrostatic energy of a $+1e$ probe charge at successive positions along the pore trajectory was then calculated using the UHBD program. Calculations were performed for each channel structure using $\epsilon_{prot} = 10$ and $I = 100$ mM. Mean electrostatic energies over all six structures and the standard deviations are reported for protonation states between 0 and 8. The order of protonation of lysine residues in a structure did not appear to greatly affect the calculated electrostatic potential profiles. Cation/anion current ratios were determined from calculated single-channel I–V curves exactly as described in Woolley et al. (1997).

RESULTS

Alamethicin K18 dimers form channels via self-assembly (Sansom, 1993b). As described previously, dimeric peptides form particular conducting structures that occur more frequently than others (Jaikaran et al., 1997). These are believed to be helix bundles composed of an even number of helices (Jaikaran et al., 1997; You et al., 1996). The particular state chosen for study in the present case is believed to be an octamer, i.e., a bundle of four dimeric peptides (Starostin et al., 1999; You et al., 1996). This state was chosen because it occurs frequently, has a lifetime sufficient for the measurement of single-channel I–V curves, and has a current large enough to permit accurate measurements of reversal potentials. Other conducting states, e.g., the putative hexamer, have qualitatively similar properties to those reported herein for the octamer. For example, Fig. 1 shows individual I–V curves for three different conducting states formed by alm-K18 at pH 7; each curve crosses the voltage axis at approximately the same point. Thus, changing the number of monomers per pore, within a limited range at least, does not appear to drastically affect cation/anion selectivity.

Cation/anion selectivity of alm-K18 is pH-dependent

Fig. 2 shows single-channel I–V relationships obtained for alm-K18 channels (octamer level) in the presence of a 0.01/1.3 M KCl gradient at pH 3.0, 7.0, 9.0, 10.3, and 11.1. The pH was the same (± 0.02 pH units) on both sides of the
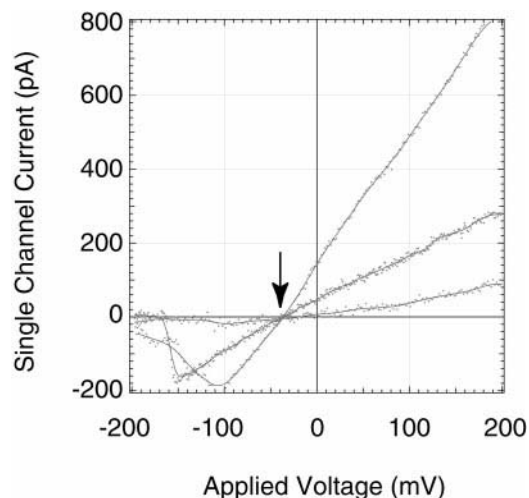
FIGURE 1 Single-channel current-voltage (I–V) curves of three different conducting states formed by alm-K18 peptides. Channels opened at $+200$ mV, whereupon the voltage was ramped to -200 mV over 30–80 ms and the current recorded. Channels closed (indicated by an abrupt change in the slope of the I–V curve) before the voltage reached -200 mV. Capacitive currents recorded when no channels opened were subtracted as described in the Experimental section. The KCl concentration was 1.3 M on the grounded side and 0.01 M on the other side with 5 mM BES, pH 7.0 on each side. Channels are oriented so that the N-terminal side is at ground. Individual examples of each conducting state are shown with a smooth line drawn through the raw data points as a visual aid only. The conducting states, from lowest to highest, are tentatively assigned as the 6-mer, 8-mer, and 10-mer, respectively. Reversal potentials (*arrow*) are approximately the same for each conducting state. Only the 8-mer state is shown in subsequent figures.

FIGURE 2   Single-channel I–V curves of the 8-mer state of alm-K18 channels recorded as described in the legend to Fig. 1, except that multiple ramps have been superimposed and closing transitions have been removed for clarity. (*A*) pH 7.0, *n* = 4 and pH 3.0, *n* = 5 superimposed; (*B*) pH 9.0, *n* = 11; (*C*) pH 10.3, *n* = 4; (*D*) pH 11.1, *n* = 9. Reversal potentials are indicated with arrows.
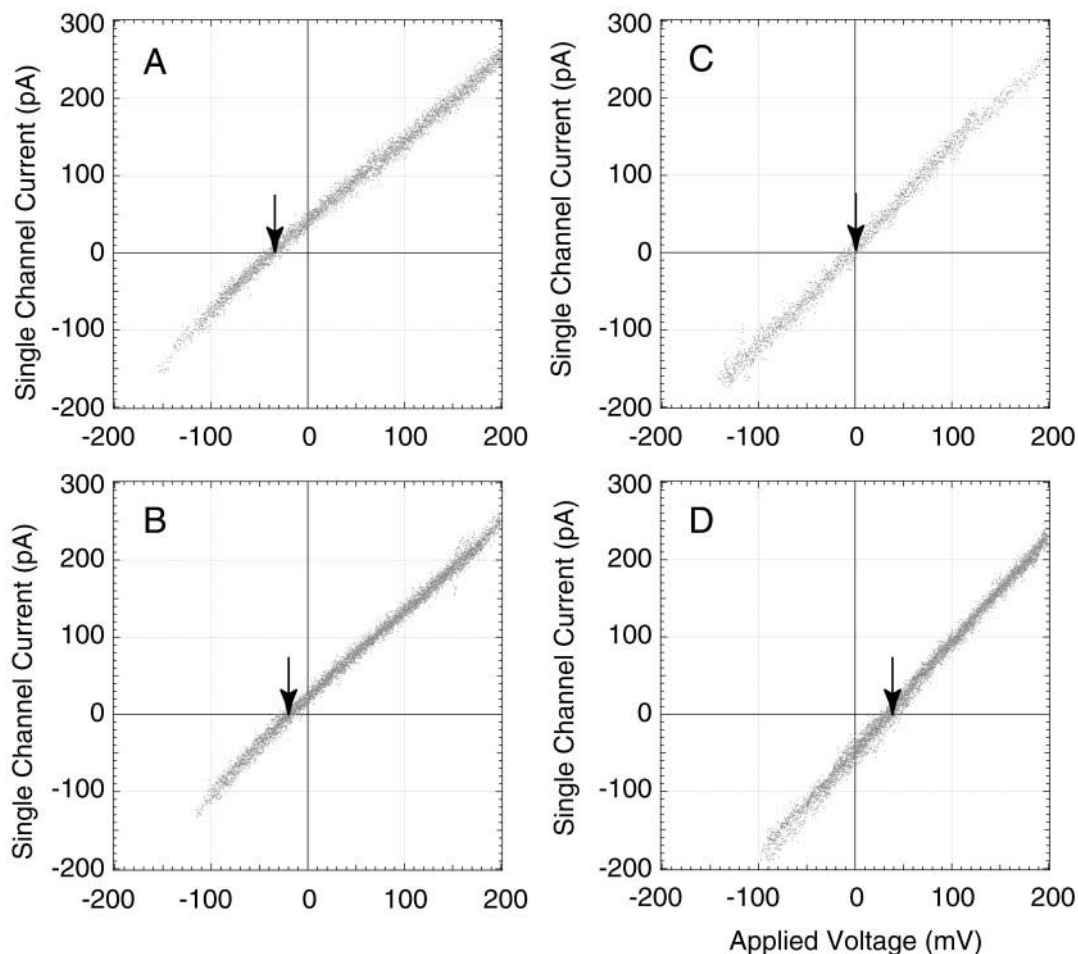
membrane. Because the high salt (1.3 M KCl) side of the membrane is at electrical ground, a negative reversal potential (ψ_{rev}), indicates a preference for chloride ions over potassium ions; likewise, a positive ψ_{rev} corresponds to cation-selectivity. Permeability ratios (P_{K^+}/P_{Cl^-}) can be estimated using Eq. 1 (Lear et al., 1997):

$$\frac{P_{K^+}}{P_{Cl^-}} = \frac{[a_{Cl^-}]_v - [a_{Cl^-}]_o \exp(\psi_{rev}F/RT)}{[a_{K^+}]_v \exp(\psi_{rev}F/RT) - [a_{K^+}]_o}, \tag{1}$$

where $[a_{K^+}]_o$ refers to the activity of K^+ ions on the ground potential side of the membrane, $[a_{K^+}]_v$ refers to the activity of K^+ ions on the opposite side, and likewise for $[a_{Cl^-}]_o$ and $[a_{Cl^-}]_v$ with respect to chloride ion activities. ψ_{rev} is the observed reversal potential and F, R, and T have their usual meanings. Activity coefficients for KCl solutions were taken from Robinson and Stokes (1968). In the case of pH 7.0 and pH 3.0, the calculated permeability ratio was $P_{K^+}/P_{Cl^-} \cong 0.25$ ($P_{Cl^-}/P_{K^+} \cong 4$). At pH 10.3, the channels were

observed to be almost non-selective with $P_{K^+}/P_{Cl^-} \cong 1$. At pH 11.1, cation-selectivity is observed with $P_{K^+}/P_{Cl^-} \cong 4$.

Fig. 3 shows I–V relationships for channels with the native alamethicin sequence (alm-Q18) measured under the same conditions as in Fig. 2. Because these channels have glutamine at position 18 in the sequence instead of lysine, they are not expected to show pH-dependent selectivity. ψ_{rev} is observed to be the same under neutral pH (7.0) and basic pH (11.1) conditions (Fig. 3). Interestingly, the ψ_{rev} of this channel is the same as that of the alm-K18 dimer channel at pH 11.1 ($P_{K^+}/P_{Cl^-} \cong 4$).

States with different cation/anion selectivities are observed at a single pH

The I–V curves shown in Fig. 2 represent those most commonly occurring at a particular pH. Although at pH 7.0 or 11.1 the most prevalent curves accounted for >90% of the total, at intermediate pH values other families of I–V
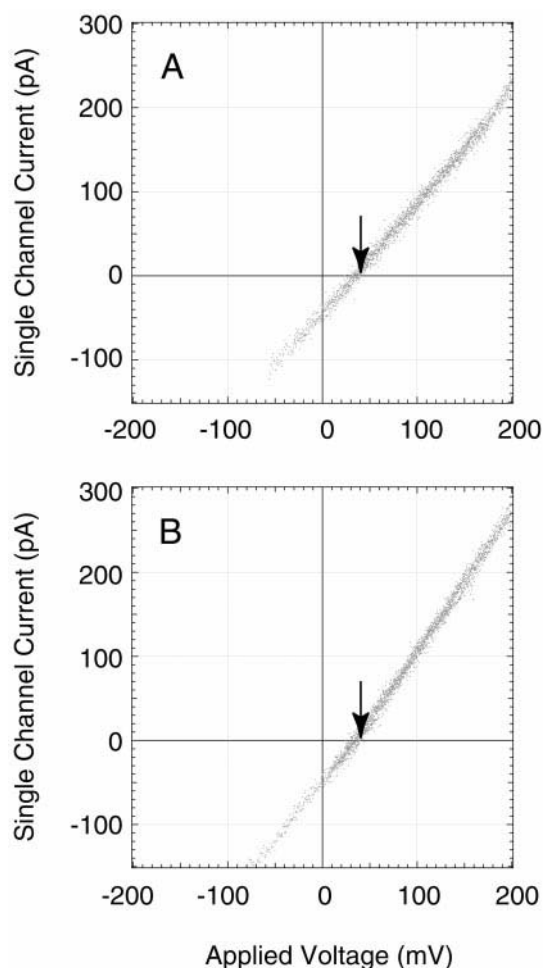
FIGURE 3 Single-channel I–V curves of the 8-mer state of alm-Q18 channels recorded as described in the legend to Fig. 2. (*A*) pH 7.0, $n = 5$; (*B*) pH 11.1, $n = 9$. Reversal potentials are indicated with arrows.

FIGURE 4 Single-channel I–V curves of the 8-mer state of alm-K18 channels recorded as described in the legend to Fig. 2. (*A*) At pH 9.55, three families of I–V curves are observed each with a different reversal potential (*arrows*); (*B*) two individual ramps are shown (pH = 9.0) in which a transition occurs that inverts selectivity. In one case the transition occurs near +25 mV; in the other case it occurs near 0 mV. From +200 mV to the transition point, an I–V curve indicative of cation-selectivity is observed (with a positive reversal potential indicated with an arrow). After the transition, an I–V curve with a negative reversal potential is observed.

curves occurred in >30% of cases. For example, at pH 9.55 three families with $\psi_{rev} \cong -15$, 0, and 15 mV were observed although the curve with $\psi_{rev} \cong -15$ mV appeared more often than others (>50% of the total) (Fig. 4 *A*). Moreover, at pH 9.0, in a few cases we were able to detect transitions between different cation/anion selectivity states during one voltage ramp. Two such transitions are represented in Fig. 4 *B*. The ramps began along a trajectory typical for a cation-selective channel, crossing the voltage axis at $\psi_{rev} = +15$ mV. Shortly thereafter, a stepwise current reversal took place; the remainder of the ramp was a trajectory typical of an anion-selective channel with a $\psi_{rev} = -15$ mV.

Macroscopic measurements of channel-forming probabilities

Alamethicin channels display a strong voltage-dependence of the macroscopic conductance as a consequence of a voltage-dependent channel formation probability (Latorre and Alvarez, 1981; Woolley and Wallace, 1992). Effects of voltage on the single-channel conductance of alm-K18 (and of alm-Q18) are minor in comparison. Dimeric forms of the peptide display similar voltage-dependent macroscopic conductance behavior (Marshall and Beusen, 1994; Woolley et

al., in preparation). The influence of different factors on channel formation probability is easiest to quantify in terms of its effect on a threshold voltage (ψ_{thr}) defined here as the voltage required to activate a conductance of 10 nS (see Hall et al., 1984; Sansom, 1991). Changes in pH are not expected to greatly alter ψ_{thr} if they do not alter channel formation probability. Native, monomeric alamethicin shows little pH dependence (Cherry et al., 1972). Likewise, the observed ψ_{thr} for alm-Q18 dimers shows negligible pH dependence (Fig. 5 *B*). With alm-K18 channels, however, there is a pronounced dependence of ψ_{thr} on pH (Fig. 5 *A*). Channel formation by alm-K18 is considerably easier at pH 11 than at pH 7, and easier at pH 7 than at pH 3.

Continuum electrostatics calculations using alm-K18 channel models

Models of octameric alm-K18 bundles were generated as described in the Experimental section. A representative model is shown in Fig. 6 with the lysine residues highlighted [prepared using the program GRASP (Nicholls et al., 1991)]. Continuum electrostatics methods were then used to calculate the effect of the protein environment on the free energies of ionization of the lysine residues in the models. Calculations were performed on six different alamethicin channel structures taken as representative of an ensemble of 25 structures generated by simulated annealing with molecular dynamics. A total of 48 lysine environments were thus sampled, with several different combinations of values for the dielectric constant of the protein and the ionic
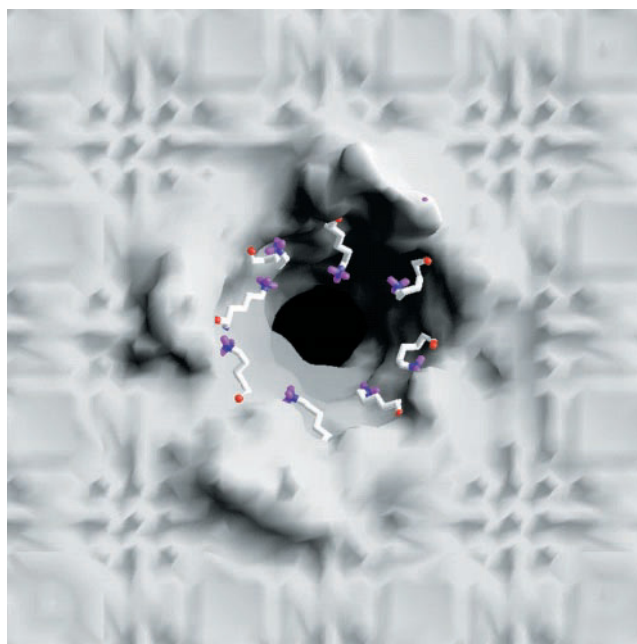
FIGURE 6   Surface representation of an octameric alm-K18 channel structure (structure # k18n8a1d1) embedded in a slab of dummy spheres to represent the low-dielectric region of the membrane. The eight lysine residues in position 18 of the sequence are show in stick representation and colored by atom type. The figure was prepared using GRASP (Nicholls et al., 1991).

strength. The calculations produce an intrinsic pK_a ($pK_a intr$) for each lysine residue and interaction energies (G_r) between all possible pairs of protonated lysine residues. The
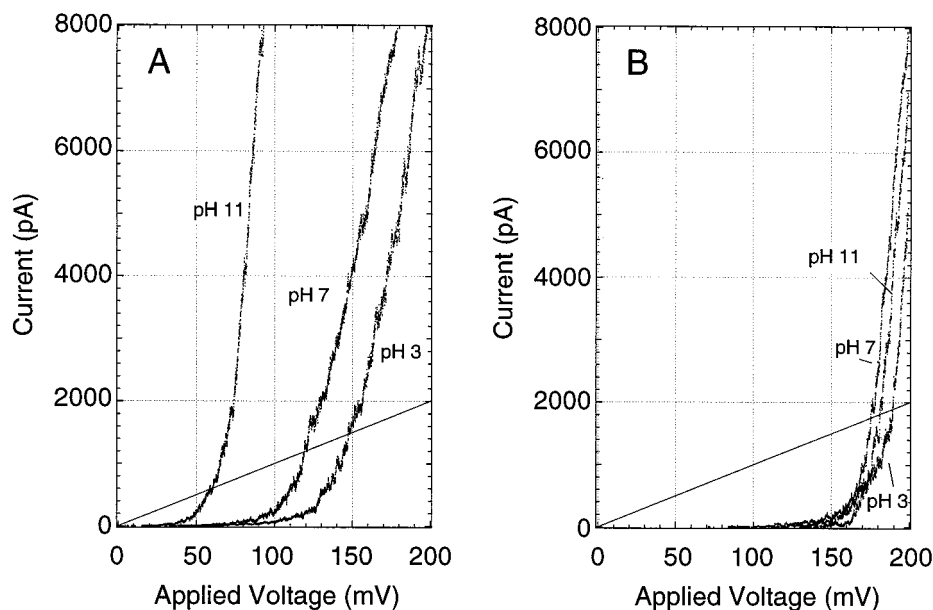
FIGURE 5   Macroscopic current observed as the voltage is raised from 0 to +200 mV over 10 s. (*A*) alm-K18, (*B*) alm-Q18. The current expected for a conductance of 10 nS is indicated with a straight line. The threshold voltage is determined by where the macroscopic current reaches the 10 nS line.

intrinsic pK_a reflects the effect of the dielectric environment and the protein partial charge distribution (assuming all other lysine residues are in their electrically neutral state) on the pK_a of the residue. The mean pK_aintr (designated $\overline{pK_a\text{intr}}$) for each channel model, and the overall mean, are reported in Table 1. The interaction energy (G_r) between two protonated lysine residues is always repulsive, but the magnitude of G_r varies considerably with the proximity of lysine pair. Mean values of G_r (designated $\overline{G_r}$) for each structure and the overall mean are reported in Table 1.

Continuum electrostatics methods were also used to calculate potential profiles for cations (and anions) along a trajectory through the pore. Trajectories and pore radius profiles were calculated using the program HOLE (Smart et al., 1993, 1997). The average pore radius profile is shown in Fig. 7 A). The radius is more variable in the C-terminal region of the channel than in the N-terminal region, largely as a result of the flexibility of the lysine residues at position 18. Electrostatic potential profiles for a cation in the modeled pore are shown in Fig. 7 B as the protonation state is increased from 0 to 8. Profiles for anions have the same magnitudes, but opposite signs. In the uncharged channel there is a barrier for cations at the N-terminus and a potential well toward the C-terminus, as observed previously for alm Q-18 (Woolley et al., 1997). As the protonation state, and thereby the assumed charge, of the lysine residues is increased, the well at the C-terminal end becomes a barrier. These potential profiles can be used to calculate approximate cation and anion currents as a function of voltage as described previously (Woolley et al., 1997). Fig. 8 shows calculated cation to anion current ratios as a function of voltage for the different electrostatic potential profiles shown in Fig. 7 B. Experimentally determined permeability ratios (determined from reversal potentials as described above) are shown for comparison.

DISCUSSION

The central experimental finding of this work is that pH affects the cation/anion selectivity of alm-K18 channels, but not of alm-Q18 channels. At low pH values (<9), alm-K18 forms anion-selective channels, whereas at high pH values, cation-selective channels are found. The effect of pH on selectivity is almost certainly due to its effect on the protonation state(s) of lysine residues in the channel. Moreover, a change in protonation state most likely alters selectivity by changing the electrostatic character, (i.e., the effective charge) of the pore. Although a change in protonation state might also affect the size of the channel and thereby selectivity, channels of a variety of sizes are typically observed to have the same selectivity at a given pH (Fig. 1). To understand how the electrostatic character of the channel affects cation/anion selectivity we now attempt to relate the pH-dependence of the selectivity (measured experimentally) to the pH dependence of channel charge calculated theoretically.

Protonation/deprotonation is expected to be fast on the time scale of an I–V measurement

The experimental measurement of cation/anion selectivity used here is the value of the reversal potential (ψ_{rev}) observed in single-channel I–V curve measurements performed in a KCl gradient. A single-channel I–V measurement (i.e., one ramp) lasts $\sim$100 ms. Let us consider how the time scale for protonation/deprotonation of lysine compares to

TABLE 1 Calculated Values of $\overline{pK_a\text{intr}}$ and $\overline{G_r}$ for Alm-K18 Channel Models

Structure Number	$\varepsilon_{prot} = 10$ $I = 0.01$ M	$\varepsilon_{prot} = 10$ $I = 0.1$ M	$\varepsilon_{prot} = 10$ $I = 1$ M	$\varepsilon_{prot} = 4$ $I = 0.1$ M	$\varepsilon_{prot} = 20$ $I = 0.1$ M
k18n8a1d1	12.09	12.02	12.03	13.03	11.58
	0.422	0.332	0.191	0.499	0.239
k18n8a1d4	11.87	11.80	11.81	12.50	11.46
	0.485	0.396	0.256	0.660	0.271
k18n8a2d2	11.96	11.89	11.90	12.65	11.52
	0.510	0.438	0.289	0.721	0.292
k18n8a3d2	11.81	11.73	11.73	12.35	11.42
	0.393	0.307	0.179	0.478	0.218
k18n8a3d3	12.60	12.52	12.54	14.13	11.85
	0.506	0.428	0.283	0.722	0.286
k18n8a4d1	12.04	11.97	11.97	12.98	11.56
	0.467	0.386	0.248	0.627	0.266
$\overline{pK_a\text{intr}}$ (overall $\pm$ SEM)	12.1 $\pm$ 0.1	11.9 $\pm$ 0.1	12.0 $\pm$ 0.1	12.9 $\pm$ 0.3	11.6 $\pm$ .1
$\overline{G_r}$ (overall $\pm$ SEM)	0.46 $\pm$ 0.02	0.38 $\pm$ 0.02	0.24 $\pm$ 0.02	0.62 $\pm$ 0.05	0.26 $\pm$ 0.01

The first value in each cell is the calculated mean pK_aintr for that structure; the second value is the mean G_r in units of kcal/mol for that structure. The bottom two rows contain mean values over all six structures (48 $pK_{a_{intr}}$ values and 168 G_r values).
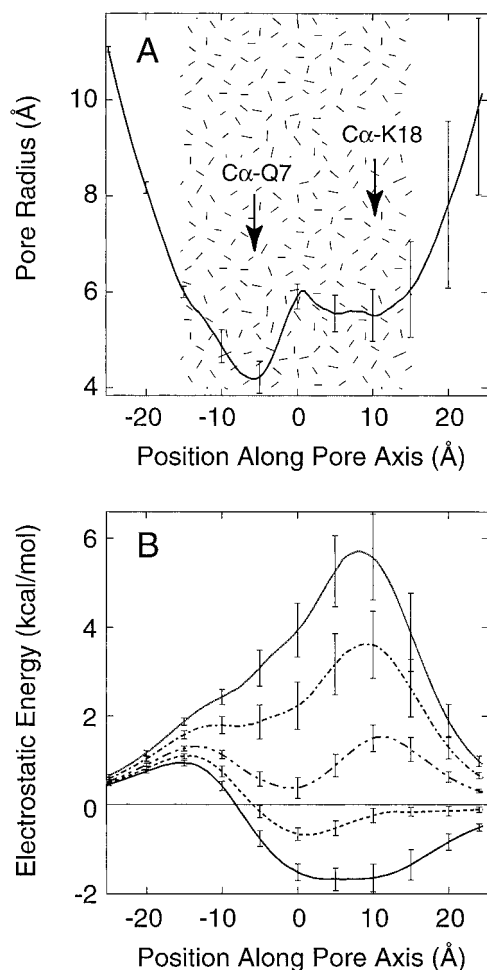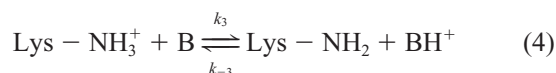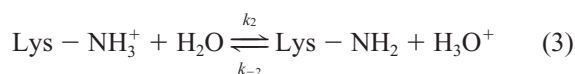
FIGURE 7 (A) Average pore radius profile of the six alm-k18 octamer models as calculated using HOLE (Smart et al., 1997). Standard deviations are indicated. The extent of the low dielectric slab is indicated by the stippled area. Approximate positions of residues Gln-7 and Lys-18 are indicated. (B) Calculated mean electrostatic potential energy of a +1e test charge as a function of position along the pore trajectory (with standard deviation shown). Charge states are: (0) ——; (+2) - - -; (+4) – – – –; (+6) – - –; (+8) ····.

this. The deprotonation of lysine may occur via any of the following mechanisms (each of which might involve extra water molecule participants; Bell, 1973; B refers to the buffer).

$$Lys - NH_3^+ + OH^- \underset{k_{-1}}{\overset{k_1}{\rightleftharpoons}} Lys - NH_2 + H_2O \qquad (2)$$

$$Lys - NH_3^+ + H_2O \underset{k_{-2}}{\overset{k_2}{\rightleftharpoons}} Lys - NH_2 + H_3O^+ \qquad (3)$$

$$Lys - NH_3^+ + B \underset{k_{-3}}{\overset{k_3}{\rightleftharpoons}} Lys - NH_2 + BH^+ \qquad (4)$$
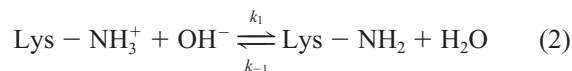
Proton transfer in the thermodynamically favorable direction is expected to be diffusion-controlled with a rate constant $k = 10^{10}$ $M^{-1}s^{-1}$ at 25°C and smaller by a factor
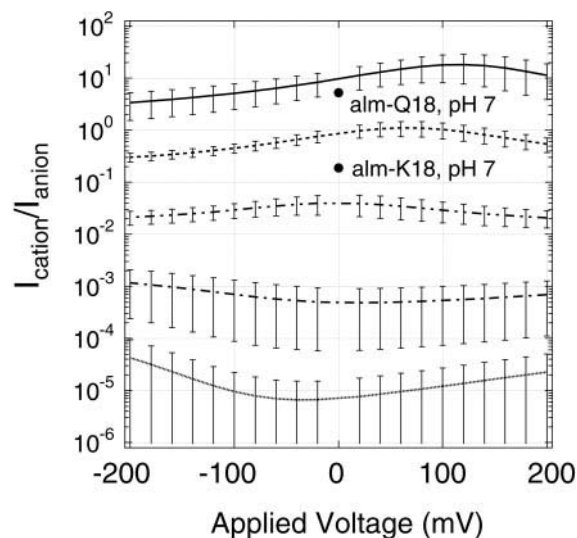
FIGURE 8 Calculated ratio of cation to anion current as a function of voltage for the different charge states shown in Fig. 7 B. Charge states are: (0) ——; (+2) - - -; (+4) – – – –; (+6) – – –; (+8) ····. Experimentally determined cation to anion permeability ratios for alm-Q18 and alm-K18 are also indicated.

ΔpK_a in the reverse direction (where ΔpK_a is the difference in the pK_a values of the partners exchanging a proton) (Bell, 1973; Eigen, 1964). If we take $pK_aLys = 10.5$ for an unperturbed lysine (and $pK_aH_2O = 15.75$; $pK_aH_3O^+ = -1.75$ (Bell, 1973, pp. 127, 128), then the forward and reverse rate constants can be calculated for processes 2 and 3 above: $k_1 = 10^{10}$ $M^{-1}s^{-1}$, $k_{-1} = 5.6 \times 10^4$ $M^{-1}s^{-1}$; $k_2 = 5.6 \times 10^{-3}$ $M^{-1}s^{-1}$, $k_{-2} = 10^{10}$ $M^{-1}s^{-1}$. The rate constants for process 4 will depend on the nature of the buffer. For CAPS ($pK_a = 10.4$) for example, k_3 and k_{-3} are expected to be on the order of 10^8 $M^{-1}s^{-1}$(Bell, 1973).

The lifetime of a protonated lysine is simply the reciprocal of the sum of the effective rate constants for the processes causing deprotonation. At pH 10, for example, $[H_3O^+] = 10^{-10}$ M, $[OH^-] = 10^{-4}$ M, $[H_2O] = 55$ M, and $[B] = 2.5 \times 10^{-3}$ M, so that the effective rate constants are 10^6 s^{-1}, 0.31 s^{-1}, and 2.5×10^5 s^{-1} for processes 2–4, respectively. The average lifetime of a protonated lysine at pH 10 is thus $1/(10^6 + 0.31 + 2.5 \times 10^5) = 8 \times 10^{-7}$ s. Similarly, one can estimate lifetimes of ~10 μs at pH 9 and 100 μs at pH 8 in the absence of buffer catalysis and ~10 times shorter in its presence. If the effective pK_a of the lysine group in question is perturbed by its environment so that is lower or higher than 10.5, the lifetime of the protonated species should still be on the order of 1–10 μs at pH 9–10, because OH^- is the strongest base in the system and the lifetime is primarily set by process 2 above.

Hydrogen bonding could extend these lifetimes significantly. For instance, the rate constant for the reaction of OH^- with (internally H-bonded) N,N-dimethylanthranilic acid (pK_a 8.4) is 1000 times slower than for the reaction of

OH$^-$ with simple amines (Eigen, 1964). Thus, conceivably, in a highly hydrogen-bonded environment with little buffer catalysis, the lifetimes of a protonated lysine might approach 1–10 ms at pH 9–10. Several groups (Kasianowicz and Bezrukov, 1995; Prod'hom et al., 1987; Root and MacKinnon, 1994) have reported single-channel measurements of elementary protonation/deprotonation reactions in a variety of protein ion channel preparations. In favorable cases, at pH values close to neutral and with D$_2$O substituting for H$_2$O, individual charged states were observed to have maximum lifetimes on the order of 1 ms. Even this lifetime is significantly shorter than the >100 ms required for an I–V measurement in the present case.

In the absence of any compelling evidence to the contrary then, we assume for the following discussion that the rate of protonation/deprotonation of lysine residues in the alm-K18 channel is fast on the time scale of an I–V measurement. Furthermore, let us assume that side-chain motion is rapid on the time scale of an I–V curve measurement, as expected from molecular dynamics simulations (Tieleman et al., 1999a,b). As lysine side chains move in the channel their pK$_a$ values will change and protonation/deprotonation events will occur. Making this assumption, individual lysine side chains are indistinguishable and what matters, from the point of view of channel selectivity, is the average charge on the ensemble of (eight) lysines. This charge, constant on the time scale of an I–V curve measurement, will depend on the pH of the solution and the effective pK$_a$ values of the residues.

Note that if one assumes protonation/deprotonation is fast on the time scale of an I–V measurement, then it follows that the protonation state being observed is an equilibrium one. That is, one cannot argue that transiently occurring uncharged or partially charged helix bundles (that are part of an equilibrium distribution) are the only channels observed.

Calculation of effective pK$_a$ values from the channel models

In an effort to gain further insight into the protonation behavior of the alm-K18 channel, we applied continuum electrostatic methods to calculate pK$_a$ values. To calculate the effective pK$_a$ values of the lysine residues in the channel, three factors need to be considered: 1) the effect of the local dielectric environment and the (non-titratable) protein charge distribution, which determines the intrinsic pK$_a$ of a lysine residue in the channel; 2) statistical effects arising from the presence of multiple indistinguishable sites; and 3) the effect of electrostatic interactions between protonated lysine residues.

The calculation of intrinsic pK$_a$ values (pK$_a$intr) was described above and calculated average values are collected in Table 1. Because lysine residues are sampling many environments on the time scale of an I–V measurement, and

the residues are indistinguishable, each lysine in the channel is assigned the same pK$_a$intr, equal to the average value, i.e., $\overline{\text{pK}_a\text{intr}}$. To address statistical effects (factor 2 above), we can define a series of pK$_a$ values that distinguish channels with different numbers of protons; for a channel with eight lysines we have:

$$\text{pK}_a1 = -\log(\text{K}_a1) \quad \text{where } \text{K}_a1 = [\text{C}_0][\text{H}^+]/[\text{C}_{1+}], \quad (5)$$

$$\text{pK}_a2 = -\log(\text{K}_a2) \quad \text{where } \text{K}_a2 = [\text{C}_{1+}][\text{H}^+]/[\text{C}_{2+}], \quad (6)$$

$$\vdots \qquad\qquad\qquad\qquad\qquad \vdots$$

$$\text{pK}_a8 = -\log(\text{K}_a8) \quad \text{where } \text{K}_a8 = [\text{C}_{7+}][\text{H}^+]/[\text{C}_{8+}], \quad (12)$$

and C$_0$ refers to uncharged channels, C$_{1+}$ to channels with one protonated lysine (at any site), etc. In general, there are Ω_i distinct ways to put i protons on eight sites (Cantor and Schimmel, 1980) where:

$$\Omega_i = \frac{8!}{(8-i)!\, i!} \quad (\text{and } \Omega_0 = \Omega_8 = 1). \quad (13)$$

As a result, the pK$_a$ values (pK$_a$1–pK$_a$8) will differ from the intrinsic $\overline{\text{pK}_a\text{intr}}$ so that:

$$\text{pK}_a i = \overline{\text{pK}_a\text{intr}} - \log\left(\frac{\Omega_{i-1}}{\Omega_i}\right) \quad (1 \le i \le 8) \quad (14)$$

Finally, electrostatic repulsion between charged lysine residues would be expected to lower the pK$_a$ values further. To estimate the magnitude of this effect we used the UHBD program to calculate the average electrostatic interaction ($\overline{G_r}$) between a pair of protonated lysine residues in the six different channel models. Let us assume that interaction energies are additive; that is, if a third proton joins a channel with two protonated lysines, two new repulsive interactions are generated. One can thus write (Cantor and Schimmel, 1980):

$$\text{pK}_a i = \overline{\text{pK}_a\text{intr}} - \log\left(\frac{\Omega_{i-1}}{\Omega}\right) - \frac{(i-1)\overline{G_r}}{2.303RT}$$

$$(1 \le i \le 8). \quad (15)$$

Calculated values of pK$_a$ (pK$_a$1–pK$_a$8) with various combinations of $\overline{\text{pK}_a\text{intr}}$ and $\overline{G_r}$ are compiled in Table 2. pK$_a$ values of several macrocyclic polyammonium compounds measured by direct potentiometric titration are collected in Table 3. The calculated effective pK$_a$ values can be used with Eqs. 5–12 to calculate the relative concentrations of each of the different protonated channel species and the average total charge on lysine residues in a channel as a function of pH. This charge can be taken to reflect the instantaneous average charge over a large number of channels or the time-average charge on one channel.

TABLE 2 Calculated pK_a Values Using $\overline{pK_a intr}$ and $\overline{G}_r$ Parameters from Table 1

Parameters	pK_a1	pK_a2	pK_a3	pK_a4	pK_a5	pK_a6	pK_a7	pK_a8
$\overline{pK_a intr}$ = 12.1 $\overline{G}_r$ = 0.46	13.00	12.30	11.71	11.17	10.64	10.09	9.51	8.83
$\overline{pK_a intr}$ = 11.9 $\overline{G}_r$ = 0.38	12.80	12.16	11.63	11.15	10.67	10.19	9.67	9.02
$\overline{pK_a intr}$ = 12.0 $\overline{G}_r$ = 0.24	12.90	12.36	11.94	11.56	11.19	10.81	10.38	9.85
$\overline{pK_a intr}$ = 12.9 $\overline{G}_r$ = 0.62	13.80	12.98	12.28	11.61	10.96	10.30	9.60	8.78
$\overline{pK_a intr}$ = 11.6 $\overline{G}_r$ = 0.26	12.50	11.95	11.51	11.11	10.73	10.33	9.90	9.34
$\overline{pK_a intr}$ = 10.5 $\overline{G}_r$ = 0.4	11.40	10.74	10.21	9.70	9.21	8.71	8.18	7.52

Units of $\overline{G}_r$ are kcal/mol.

Comparison of calculations with experiment

Because the observed single-channel selectivity of alm-K18 at pH 11.1 is similar to that of alm-Q18, which is formally uncharged, it is unlikely that alm-K18 bears significant positive charge at pH 11.1. Thus, the single-channel selectivity measurements suggest that no pK_a of the channel is higher than ~11. The highest pK_a values (pK_a1) for the macrocyclic model compounds (Table 3) are ~10.5 unless there is a vicinal oxygen atom in the structure, in which case the maximum pK_a is lower [viz. ethylamine (pK_a = 10.64) vs. ethanolamine (pK_a = 9.5) (Weast and Astle, 1981)].

The highest pK_a (i.e., pK_a1) depends primarily on the value of $\overline{pK_a intr}$, not on $\overline{G}_r$. Values calculated for pK_a1 in the alamethicin models are all higher than 11. The accuracy of the calculated values for $\overline{pK_a intr}$ depend, of course, on the degree to which the model structures reflect the actual structures and the appropriateness of the continuum dielectric representation of the electrostatics. The $\overline{pK_a intr}$ of an unperturbed lysine residue is 10.5. A higher pK_a implies that the local protein environment stabilizes the positively charged form of lysine. In the present case, the effect is presumably due to a favorable interaction of the positive charge with the C-terminal end of the alamethicin helix dipoles. Helix dipoles have been shown experimentally (Huyghues-Despointes et al., 1993) and theoretically (Adcock et al., 1998; Sitkoff et al., 1994) to have strong effects on the pK_a values of attached residues. An overestimate for $\overline{pK_a intr}$ may be a consequence of side-chain mobility, as has been suggested by others (Antosiewicz et al., 1994; Honig et al., 1993; van Vlijmen et al., 1998), although the aver-
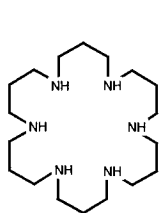
TABLE 3 Experimentally Determined pK_a Values for Model Compounds

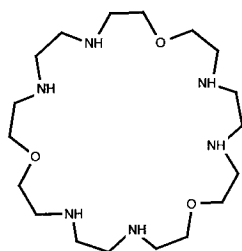| Structure	pK_a1	pK_a2	pK_a3	pK_a4	pK_a5	pK_a6	pK_a7	pK_a8
1*	10.45	10.35	9.05	7.90	7.15	6.60		
2*	9.65	9.15	8.45	6.80	5.80	5.70		
3*	10.70	10.45	9.65	9.00	8.05	7.50	6.95	6.45
4†	8.75	7.98	7.46	7.19	6.64	6.62	5.49	

*Data from (Dietrich et al., 1981).
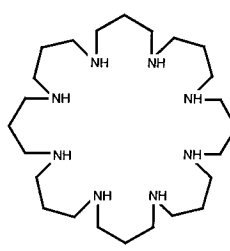†Data from (O'Keeffe et al., 1997).
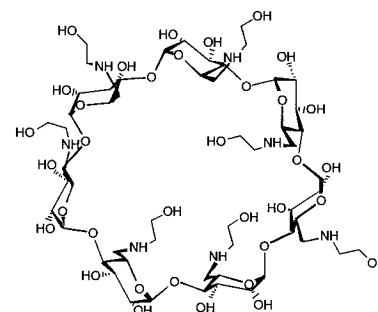pK_a Values were measured in aqueous solution with an ionic strength of 100 mM.

1   **2**   **3**   **4**

aging of the calculated $\overline{pK_a intr}$ over many side-chain conformations might have been expected to correct for this deficiency. Alternatively, the electrostatic consequences of a partially ordered water structure in the pore, which would reduce the helix dipole by introducing an opposing channel water dipole (Breed, 1996), may need to be considered in the $pK_a intr$ calculation.

The value of the lowest pK_a depends on the intrinsic pK_a, the size of the interaction energy, and the number of titratable sites. The difference between the highest and lowest pK_a values, however, depends primarily on the interaction energy ($\overline{G_r}$) between sites. Each of the macrocyclic model compounds listed in Table 3 exhibits a difference of between 3–4 pH units between the highest and lowest pK_a values. Interaction energies calculated for the alamethicin model channels vary from ~0.25 to 0.6 kcal/mol, depending on the choice of ϵ_{prot} and I. A value in the middle of this range, e.g., 0.4 kcal/mol, also predicts a pK_a range of 3–4 pH units (see Table 2, bottom row). The model compounds are somewhat smaller than the alamethicin bundle so that distances between protonated sites would be lower, and interaction energies higher than in the channel. However, the partially hydrophobic environment of the lysine residues in the channel, as compared to the model compounds, would tend to raise the value of $\overline{G_r}$ in the channel. A difference of 3–4 pH units between the highest and lowest pK_a values in the alm-K18 channel would be broadly consistent with pK_a ranges measured by direct potentiometric titration of model compounds.

The observation that the single-channel selectivity does not change as the pH is lowered below 7.0 (Fig. 2) is also consistent with no pK_a in the channel being below 7.0. The macroscopic current measurements shown in Fig. 5 indicate that the voltage required to obtain given current with alm-K18 increases as the pH is lowered from pH 11 to pH 7 and from pH 7 to pH 3. The observed current is believed to reflect primarily channel formation probability (Sansom, 1993b) which requires membrane insertion and aggregation of alm-K18 peptides (Cafiso, 1994; Sansom, 1993b; Woolley and Wallace, 1992). It is reasonable to expect that as the degree of protonation of the lysine residues increases, electrostatic repulsion hinders the channel formation process. Because the threshold voltage increases as the pH is lowered from pH 7 to pH 3, one would conclude that some lysine residues have pK_a values below pH 7. However, an alm-K18 aggregate (e.g., a tetramer) involved in macroscopic current generation may be responsible for this pK_a, not necessarily the putative octameric state under study in the single-channel experiments.

Origin of states with different cation/anion selectivities at a single pH

It remains to explain the origin of the different selectivities observed in single-channel I–V measurements at pH values between 8.5 and 10. Inasmuch as these different selectivities interconvert only rarely over the time course of an I–V measurement (Fig. 4), they must reflect states with intrinsic lifetimes >100 ms or so. This time scale is significantly longer than that expected for an elementary protonation or deprotonation event, as discussed above.

Because the states have different selectivities, it is likely they have different effective charges and different degrees of protonation. If protonation is fast, then different degrees of protonation must result from changes in effective pK_a values on the 100-ms time scale (or slower). Such changes could presumably arise from conformational fluctuations in the alm-K18 helix bundle. Different helix packing arrangements are seen in octamer bundles generated using simulated annealing with molecular dynamics; perhaps some of these interconvert slowly. Different conformers would have slightly different $\overline{pK_a intr}$ and $\overline{G_r}$ values (see Table 1) and therefore different effective pK_a values. Alm-K18 helix bundles with slightly different effective pK_a values will differ most in their effective charges in the mid-range of their titration curves, i.e., between 8.5 and 10.

Protonation state, effective charge and cation/anion selectivity

If a particular charge state is assumed, one can use the UHBD program to calculate an electrostatic potential energy profile for a cation or anion as it moves through the pore. Because the calculation is approximate and cannot rigorously deal with a salt concentration gradient, intermediate values of ϵ_{prot} and I were assumed. These profiles (Fig. 7 B) were combined with a linear applied voltage term to approximate the voltage as a function of position in the channel. This description was then used with the Nernst-Planck equation to predict I–V curves as described previously (Woolley et al., 1997). Although approximate, this calculation gives an estimate of the relative current carried by cations and anions as the electrostatic profile of the channel is changed (Dieckmann et al., 1999; Woolley et al., 1997). Because the average lifetime of the protonated state of a lysine residue in the channel (with a pKa between 7 and 12, see above) is likely to be longer than the average residence time of an ion in the channel (1–100 ns), increases in the charge state were simulated by fully protonating individual lysines in the bundle. Thus, a charge state of two means that two lysines have one full charge each, not that each lysine of the eight has 0.25 charge.

Fig. 8 shows cation/anion current ratios calculated in this manner. A net channel charge of zero reproduces reasonably well the cation/anion selectivity determined from reversal potential measurements for alm-K18 at high pH and for alm-Q18 at all pH values. As the charge state of the channel increases, the calculation correctly predicts a switch in selectivity from cationic to anionic. An effective charge of ~3+ to 4+ reproduces the observed cation/anion selectiv-

ity of the alm-K18 channel at pH 7 and below. If eight charges are placed in the channel, however, extreme anion-selectivity is predicted. In a preliminary report of this work (Starostin et al., 1999), we concluded that at pH 7.0, the effective charge on the channel is approximately four. However, the arguments presented above lead one to the conclusion that the channel is in fact fully protonated at pH 7.0. Thus, it would appear that the electrostatic calculation overestimates the effective charge sensed by a permeant cation if positive charges are simply added to lysines in the structure. The size of this disagreement indicates that either the modeled structure is inappropriate or that the calculations fail to capture some important aspect of the permeation process, or both. Because the modeled structure appears sufficient to explain the properties of native alamethicin channels and the titration behavior of alm-K18, let us consider possible deficiencies in the continuum electrostatic description of permeation.

One possible cause of the overestimation of selectivity is that the lysine conformations in the models do not adequately reflect the experimental situation even though a variety of lysine conformations are sampled through averaging of the electrostatic energy profiles (van Vlijmen et al., 1998). Models were generated in vacuo assuming a partial charge of 0.4 for the lysine side chains. However, the average lysine side-chain conformation may in fact change as the degree of protonation increases. We are currently investigating the effect of protonation state on lysine side-chain conformations using all-atom molecular dynamics simulations.

Another possibility is that permeating ions may perturb the conformational states of the lysine side chains. The flexibility of these side chains is such that the position of the charged amino groups may change appreciably on the time scale of permeation. Likewise, the positions of the lysines may alter the path of a permeant ion so that the trajectory calculated using the HOLE program is inappropriate. The trajectory favored by anions may be different from that of cations. It is also conceivable that a permeating cation could approach a side chain so closely as to cause a dramatic alteration in the side-chain pKa and trigger a deprotonation event. Such an effect is difficult to reproduce in a continuum theory, but might be expected to increase P_{K^+}/P_{Cl^-} in the protonated channel. The relative importance of such a process may be addressed by constructing alm-K18 channels in which the lysine side-chain amino groups are replaced by non-ionizable quaternary ammonium groups.

A final possible cause of an overestimation of the selectivity is that the ring of lysine residues, when protonated, might bind a counterion (e.g., Cl^-) tightly. If a counterion binds as a consequence of a protonation event, the effective charge of the channel has not increased. Thus, there may be a disconnection between titration (protonation) and increasing effective charge, particularly in the lower pH range where most of the lysines are protonated. Molecular dynam-

ics simulations at different effective ionic strengths may help address this issue (Pfeiffer et al., 1999).

If counterion binding to charged side chains is indeed significant, it may set an inherent limit on the degree of cation/anion selectivity obtainable via a simple electrostatic mechanism, at least in a relatively wide channel. In a wide channel, either K^+ or Cl^- could simply bypass a lysine-counterion pair. This suggestion recalls that proposed by Borisova et al. (1986) to explain cation/anion selectivity properties of channels formed by amphotericin B. A role for bound counterions has also been proposed by Franciolini and Nonner (1987) in describing permeation through a neuronal anion channel. Perhaps higher degrees of anion-selectivity require a channel to control the path of ions so that permeation requires displacement of a lysine-counterion (or some other side chain-anion pair).

The preceding discussion has highlighted several possible features of permeation that would be overlooked with the continuum electrostatic approach as it is used here. The analysis is useful in so far as it provides a list of features that may be important as a focus for further study. It is hoped that an all-atom molecular dynamics treatment, currently in progress, might enable a better description of the electrostatics of permeation in the alm-K18 channel.

REFERENCES

Adcock, C., G. R. Smith, and M. S. P. Sansom. 1998. Electrostatics and the ion selectivity of ligand-gated channels. *Biophys. J.* 75:1211–1222.

Antosiewicz, J., J. A. McCammon, and M. K. Gilson. 1994. Prediction of pH-dependent properties of proteins. *J. Mol. Biol.* 238:415–436.

Bashford, D., and M. Karplus. 1990. pKa's of ionizable groups in proteins: atomic detail from a continuum electrostatic model. *Biochemistry.* 29:10219–10225.

Bell, R. P. 1973. The Proton in Chemistry. Cornell University Press, Ithaca, New York.

Bell, T. W. 1998. Carriers and channels: current progress and future prospects. *Curr. Opin. Chem. Biol.* 2:711–716.

Boerrigter, H., L. Grave, J. Nissink, L. Chrisstoffels, J. van der Maas, W. Verboom, F. de Jong, and D. Reinhoudt. 1998. (Thio)urea resorcinarene cavitands. Complexation and membrane transport of halide anions. *J. Org. Chem.* 63:4174–4180.

Borisova, M. P., R. A. Brutyan, and L. N. Ermishkin. 1986. Mechanism of anion-cation selectivity of amphotericin B channels. *J. Membr. Biol.* 90:13–20.

Bowen, K. A., K. Tam, and M. Colombini. 1985. Evidence for titratable gating charges controlling the voltage dependence of the outer mitochondrial membrane channel, VDAC. *J. Membr. Biol.* 86:51–9.

Breed, J. 1996. Molecular Modelling of Ion Channels. Oxford University.

Breed, J., P. C. Biggin, I. D. Kerr, O. S. Smart, and M. S. P. Sansom. 1997. Alamethicin channels: modeling via restrained molecular dynamics simulations. *Biochim. Biophys. Acta.* 1325:235–249.

Brooks, B. R., R. E. Bruccoleri, B. D. Olafson, D. J. States, S. Swaminathan, and M. Karplus. 1983. CHARMM: a program for macromolec-

ular energy minimization and dynamics calculations. *J. Comp. Chem.* 4:187–217.

Brunger, A. T. 1992. X-PLOR Version 3.1. A System for X-ray Crystallography and NMR. Yale University Press, New Haven, CT.

Cafiso, D. S. 1994. Alamethicin: a peptide model for voltage gating and protein-membrane interactions. *Annu. Rev. Biophys. Biomol. Struct.* 23:141–165.

Cantor, C. R., and P. R. Schimmel. 1980. Biophysical Chemistry, Part III: The Behavior of Biological Macromolecules. W. H. Freeman, San Francisco.

Cescatti, L., C. Pederzolli, and G. Menestrina. 1991. Modification of lysine residues of *Staphylococcus aureus* alpha-toxin: effects on its channel-forming properties. *J. Membr. Biol.* 119:53–64.

Cherry, R. J., D. Chapman, and D. E. Graham. 1972. Studies of the conductance changes induced in bimolecular lipid membranes by alamethicin. *J. Membr. Biol.* 7:325–344.

Corringer, P. J., S. Bertrand, J. L. Galzi, A. Devillers-Thiery, J. P. Changeux, and D. Bertrand. 1999. Mutational analysis of the charge selectivity filter of the alpha7 nicotinic acetylcholine receptor. *Neuron.* 22: 831–843.

Cox, B., G. Hedwig, A. Parker, and D. Watts. 1974. Solvation of ions. XIX. Thermodynamic properties for transfer of single ions between protic and dipolar aprotic solvents. *Aust. J. Chem.* 27:477–501.

Darveau, R. P., R. E. Hancock, and R. Benz. 1984. Chemical modification of the anion selectivity of the PhoE porin from the *Escherichia coli* outer membrane. *Biochim. Biophys. Acta.* 774:67–74.

Davis, M. E., J. D. Madura, B. A. Luty, and J. A. McCammon. 1991. Electrostatics and diffusion of molecules in solution: simulations with the University of Houston Brownian dynamics program. *Comput. Phys. Comm.* 62:187–197.

Dieckmann, G. R., J. D. Lear, Q. Zhong, M. Klein, M. L. DeGrado, and K. A. Sharp. 1999. Exploration of the structural features defining the conduction properties of a synthetic channel. *Biophys. J.* 76:618–630.

Dietrich, B., M. W. Hosseini, J. M. Lehn, and R. B. Sessions. 1981. Anion receptor molecules. Synthesis and anion-binding properties of polyammonium macrocycles. *J. Am. Chem. Soc.* 103:1282–1283.

Dorman, V., M. B. Partenskii, and P. C. Jordan. 1996. A semi-microscopic Monte Carlo study of permeation energetics in a gramicidin-like channel: the origin of cation selectivity. *Biophys. J.* 70:121–134.

Doyle, D. A., J. Morais Cabral, R. A. Pfuetzner, A. Kuo, J. M. Gulbis, S. L. Cohen, B. T. Chait, and R. MacKinnon. 1998. The structure of the potassium channel: molecular basis of K^+ conduction and selectivity. *Science.* 280:69–77.

Dutzler, R., G. Rummel, S. Alberti, S. Hernandez-Alles, P. Phale, J. Rosenbusch, V. Benedi, and T. Schirmer. 1999. Crystal structure and functional characterization of ompK36, the osmoporin of *Klebsiella pneumoniae*. *Structure.* 7:425–434.

Eigen, M. 1964. Proton transfer, acid-base catalysis, and enzymatic hydrolysis. *Angew. Chem. Intl. Ed.* 3:1–72.

Fahlke, C., H. T. Yu, C. L. Beck, T. H. Rhodes, and A. L. George, Jr. 1997. Pore-forming segments in voltage-gated chloride channels. *Nature.* 390: 529–532.

Franciolini, F., and W. Nonner. 1987. Anion and cation permeability of a chloride channel in rat hippocampal neurons. *J. Gen. Physiol.* 90: 453–478.

Guinamard, R., and M. H. Akabas. 1999. Arg352 is a major determinant of charge selectivity in the cystic fibrosis transmembrane conductance regulator chloride channel. *Biochemistry.* 38:5528–5537.

Hall, J. E., I. Vodyanoy, T. M. Balasubramanian, and G. R. Marshall. 1984. Alamethicin: a rich model for channel behavior. *Biophys. J.* 45:233–248.

Hancock, R. E., and R. Benz. 1986. Demonstration and chemical modification of a specific phosphate binding site in the phosphate-starvation-inducible outer membrane porin protein P of *Pseudomonas aeruginosa*. *Biochim. Biophys. Acta.* 860:699–707.

Honig, B., and A. Nicholls. 1995. Classical electrostatics in biology and chemistry. *Science.* 268:1144–1149.

Honig, B., K. Sharp, and A. Yang. 1993. Macroscopic models of aqueous solutions: biological and chemical applications. *J. Phys. Chem.* 97: 1101–1109.

Huyghues-Despointes, B. M., J. M. Scholtz, and R. L. Baldwin. 1993. Effect of a single aspartate on helix stability at different positions in a neutral alanine-based peptide. *Protein Sci.* 2:1604–1611.

Jaikaran, D. C., P. C. Biggin, H. Wenschuh, M. S. P. Sansom, and G. A. Woolley. 1997. Structure-function relationships in helix-bundle channels probed via total chemical synthesis of alamethicin dimers: effects of a Gln^7 to Asn^7 mutation. *Biochemistry.* 36:13873–13881.

Karshikoff, A., V. Spassov, S. W. Cowan, R. Ladenstein, and T. Schirmer. 1994. Electrostatic properties of two porin channels from *Escherichia coli*. *J. Mol. Biol.* 240:372–384.

Kasianowicz, J. J., and S. M. Bezrukov. 1995. Protonation dynamics of the alpha-toxin ion channel from spectral analysis of pH-dependent current fluctuations. *Biophys. J.* 69:94–105.

Lanyi, J. K., A. Duschl, G. Varo, and L. Zimanyi. 1990. Anion binding to the chloride pump, halorhodopsin, and its implications for the transport mechanism. *FEBS Lett.* 265:1–6.

Latorre, R., and O. Alvarez. 1981. Voltage-dependent channels in planar lipid bilayer membranes. *Physiol. Rev.* 61:77–150.

Lear, J. D., J. P. Schneider, P. K. Kienker, and W. F. DeGrado. 1997. Electrostatic effects on ion selectivity and rectification in designed ion channel peptides. *J. Am. Chem. Soc.* 119:3212–3217.

Levitt, D. G. 1991a. General continuum theory for multiion channel I. Theory. *Biophys. J.* 59:271–277.

Levitt, D. G. 1991b. General continuum theory for multiion channel II. Application to acetylcholine channel. *Biophys. J.* 59:278–288.

Malashkevich, V. N., R. A. Kammerer, V. P. Efimov, T. Schulthess, and J. Engel. 1996. The crystal structure of a five-stranded coiled coil in COMP: a prototype ion channel? *Science.* 274:761–765.

Marcus, Y. 1997. Ion Properties. Marcel Dekker, Inc., New York.

Marshall, G. R., and D. D. Beusen. 1994. The structural basis of peptide channel formation. *In* Biomembrane Electrochemistry. American Chemical Society, Washington, DC. 259–314.

Moczydlowski, E. 1998. Chemical basis for alkali cation selectivity in potassium-channel proteins. *Chem. Biol.* 5:R291–R301.

Nicholls, A., K. A. Sharp, and B. Honig. 1991. Protein folding and association: insights from the interfacial and thermodynamic properties of hydrocarbons. *Proteins.* 11:281–296.

Nilges, M., and A. T. Brunger. 1993. Successful prediction of the coiled coil geometry of the GCN4 leucine zipper domain by simulated annealing: comparison to the x-ray structure. *Proteins: Struct., Funct., Genet.* 15:133–146.

O'Keeffe, F., S. A. Shamsi, R. Darcy, P. Schwinte, and I. M. Warner. 1997. A persubstituted cationic β-cyclodextrin for chiral separations. *Anal. Chem.* 69:4773–4782.

Perutz, M. F., D. T. Shih, and D. Williamson. 1994. The chloride effect in human haemoglobin. A new kind of allosteric mechanism. *J. Mol. Biol.* 239:555–560.

Pfeiffer, S., D. Fushman, and D. Cowburn. 1999. Impact of Cl^- and Na^+ ions on simulated structure and dynamics of βARK1 PH domain. *Proteins: Struct., Funct., Genet.* 35:206–217.

Prod'hom, B., D. Pietrobon, and P. Hess. 1987. Direct measurement of proton transfer rates to a group controlling the dihydropyridine-sensitive Ca^{2+} channel. *Nature.* 329:243–246.

Rink, T., H. Bartel, G. Jung, W. Bannwarth, and G. Boheim. 1994. Effects of polycations on ion channels formed by neutral and negatively charged alamethicins. *Eur. Biophys. J.* 23:155–165.

Robinson, R. A., and R. H. Stokes. 1968. Electrolyte Solutions. Butterworths, London.

Root, M. J., and R. MacKinnon. 1994. Two identical noninteracting sites in an ion channel revealed by proton transfer. *Science.* 265:1852–1856.

Sansom, M. S. P. 1991. The biophysics of peptide models of ion channels. *Prog. Biophys. Mol. Biol.* 55:139–235.

Sansom, M. S. P. 1993a. Alamethicin and related peptaibols—model ion channels. *Eur. Biophys. J.* 22:105–124.

Sansom, M. S. P. 1993b. Structure and function of channel-forming peptaibols. *Q. Rev. Biophys.* 26:365–421.

Sansom, M. S. P. 1998. Models and simulations of ion channels and related membrane proteins. *Curr. Opin. Struct. Biol.* 8:237–244.

Schmid, B., L. Maveyraud, M. Kromer, and G. E. Schulz. 1998. Porin mutants with new channel properties. *Protein Sci.* 7:1603–1611.

Schmidtchen, F., and M. Berger. 1997. Artificial organic host molecules for anions. *Chem. Rev.* 97:1609–1646.

Sitkoff, D., D. J. Lockhart, K. A. Sharp, and B. Honig. 1994. Calculation of electrostatic effects at the amino terminus of an alpha helix. *Biophys. J.* 67:2251–2260.

Smart, O. S., J. Breed, G. R. Smith, and M. S. P. Sansom. 1997. A novel method for structure-based prediction of ion channel conductance properties. *Biophys. J.* 72:1109–1126.

Smart, O. S., J. M. Goodfellow, and B. A. Wallace. 1993. The pore dimensions of gramicidin A. *Biophys. J.* 65:2455–2460.

Starostin, A. V., R. Butan, V. Borisenko, D. A. James, H. Wenschuh, M. S. P. Sansom, and G. A. Woolley. 1999. An anion-selective analogue of the channel-forming peptide alamethicin. *Biochemistry.* 38:6144–6150.

Tabcharani, J. A., P. Linsdell, and J. W. Hanrahan. 1997. Halide permeation in wild-type and mutant cystic fibrosis transmembrane conductance regulator chloride channels. *J. Gen. Physiol.* 110:341–54.

Tieleman, D. P., H. J. Berendsen, and M. S. P. Sansom. 1999a. An alamethicin channel in a lipid bilayer: molecular dynamics simulations. *Biophys. J.* 76:1757–1769.

Tieleman, D. P., M. S. P. Sansom, and H. J. C. Berendsen. 1999b. Alamethicin helices in a bilayer and in solution: molecular dynamics simulations. *Biophys. J.* 76:40–49.

Van Gelder, P., N. Saint, R. van Boxtel, J. P. Rosenbusch, and J. Tommassen. 1997. Pore functioning of outer membrane protein PhoE of *Escherichia coli*: mutagenesis of the constriction loop L3. *Protein Eng.* 10:699–706.

van Vlijmen, H. W. T., M. Schaefer, and M. Karplus. 1998. Improving the accuracy of protein pK_a calculations: conformational averaging versus the average structure. *Proteins: Struct., Funct., Genet.* 33:145–158.

Wang, C. T., H. G. Zhang, T. A. Rocheleau, R. H. ffrench-Constant, and M. B. Jackson. 1999. Cation permeability and cation-anion interactions in a mutant GABA-gated chloride channel from *Drosophila. Biophys. J.* 77:691–700.

Warshel, A., and A. Papazyan. 1998. Electrostatic effects in macromolecules: fundamental concepts and practical modeling. *Curr. Opin. Struct. Biol.* 8:211–217.

Weast, R. C., and M. J. Astle. 1981. CRC Handbook of Chemistry and Physics. CRC Press Inc., Boca Raton, FL.

Weetman, P., S. Goldman, and C. G. Gray. 1997. Use of the Poisson-Boltzmann equation to estimate the electrostatic free energy barrier for dielectric models of biological ion channels. *J. Phys. Chem. B.* 101:6073–6078.

Woolley, G. A., P. C. Biggin, A. Schultz, L. Lien, D. C. J. Jaikaran, J. Breed, K. Crowhurst, and M. S. P. Sansom. 1997. Intrinsic rectification of ion flux in alamethicin channels: studies with an alamethicin dimer. *Biophys. J.* 73:770–778.

Woolley, G. A., and B. A. Wallace. 1992. Model ion channels: gramicidin and alamethicin. *J. Membr. Biol.* 129:109–136.

You, S., S. Peng, L. Lien, J. Breed, M. S. P. Sansom, and G. A. Woolley. 1996. Engineering stabilized ion channels: covalent dimers of alamethicin. *Biochemistry.* 35:6225–6232.